Organosilylated Complex [Eu(TTA)$_3$(Bpy-Si)]: A Bifunctional Moiety for the Engeneering of Luminescent Silica-Based Nanoparticles for Bioimaging

Adriana P. Duarte,*[,†,‡] Léïla Mauline,[†] Marie Gressier,[†] Jeannette Dexpert-Ghys,[§] Christine Roques,[∥] José Maurício A. Caiut,[⊥] Elenice Deffune,[#] Danielle C. G. Maia,[▽] Iracilda Z. Carlos,[▽] Antonio A. P. Ferreira,[‡] Sidney J. L. Ribeiro,*[,‡] and Marie-Joëlle Menu*[,†]

[†]Centre Interuniversitaire de Recherche et d'Ingénierie des Matériaux, Université de Toulouse, UPS-CNRS 5085, 118 route de Narbonne, 31062 Toulouse Cedex 9, France.

[‡]Institute of Chemistry, São Paulo State University, UNESP, CP355-Araraquara-SP, 14801-970-Brazil

[§]Centre d'Elaboration de Matériaux et d'Etudes Structurales, CNRS UPR 8011, 21 rue J. Marvig, B.P. 94347, 31055, Toulouse Cedex 4, France

[∥]Laboratoire de Génie Chimique, UMR-CNRS 5503, Université Paul Sabatier, 35 Chemin des Maraîchers, 31062 Toulouse Cedex 9, France

[⊥]Department of Chemistry, University of São Paulo, FFCLRP, Ribeirão Prêto SP, Brazil

[#]Botucatu Medical School, São Paulo State University, UNESP, Botucatu SP, 18618-970 Brazil

[▽]School of Pharmaceutical Sciences, São Paulo State University, UNESP, 14801-902 Brazil

ABSTRACT: A new highly luminescent europium complex with the formula [Eu(TTA)$_3$(Bpy-Si)], where TTA stands for the thenoyltrifluoroacetone, $(C_4H_3S)COCH_2COCF_3$, chelating ligand and Bpy-Si, Bpy-$CH_2NH(CH_2)_3Si(OEt)_3$, is an organosilyldipyridine ligand displaying a triethoxysilyl group as a grafting function has been synthesized and fully characterized. This bifunctional complex has been grafted onto the surface of dense silica nanoparticles (NPs) and on mesoporous silica microparticles as well. The covalent bonding of [Eu(TTA)$_3$(Bpy-Si)] inside uniform Stöber silica nanoparticles was also achieved. The general methodology proposed could be applied to any silica matrix, allowed high grafting ratios that overcome chelate release and the tendency to agglomerate. Luminescent silica-based nanoparticles SiO_2-[Eu(TTA)$_3$(Bpy-Si)], with a diameter of 28 ± 2 nm, were successfully tested as a luminescent labels for the imaging of *Pseudomonas aeruginosa* biofilms. They were also functionalized by a specific monoclonal antibody and subsequently employed for the selective imaging of *Escherichia coli* bacteria.

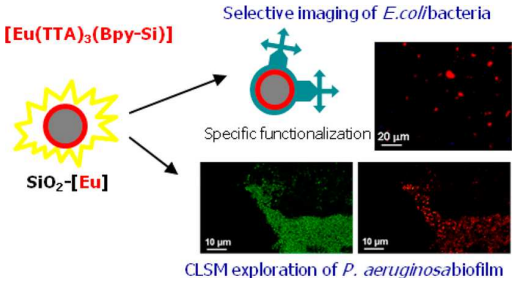

1. INTRODUCTION

Lanthanide complexes, essentially complexes of Eu^{3+} and Tb^{3+}, are an important class of compounds for the development of advanced luminescent materials with applications in lighting, optoelectronics, biological assays, and bioimaging.[1−4] In such well-chosen complexes, the low absorption of exciting light by Ln^{3+} as a result of the forbidden nature of intra-4f^n electronic transitions is circumvented by the strong absorption of the ligand, associated with an efficient intramolecular ligand to metal energy transfer: the so-called antenna effect. Several reviews devoted to lanthanide-related properties in organic−inorganic hybrid materials were reported in the last few years.[5−8] Silica-based hybrids have been developed for optoelectronic devices because of the interesting properties of silica: a large transparency domain, shape versatility, and its good thermal and mechanical resistances. The advantages inherent in silica-based nanoparticles in the biological field have been highlighted by Wang:[9] the silica shell provides an attractive environment for its stability in water, its possible surface functionalization, and its biocompatibility. Luminescent Eu^{3+} or Tb^{3+} complexes embedded in silica nanoparticles (NPs) present several advantages over more conventional organic fluorescent dyes because of their unique spectral properties: large Stokes shifts with respect to near-UV excitation and long decay times that make them suitable for microsecond time-gated luminescence imaging. This potential has been illustrated by the use of bioconjugated silica nanoparticles embedding an europium complex to perform

Scheme 1. Schematical Representation of the Methodologies Employed to Obtain Luminescent Particles[a]

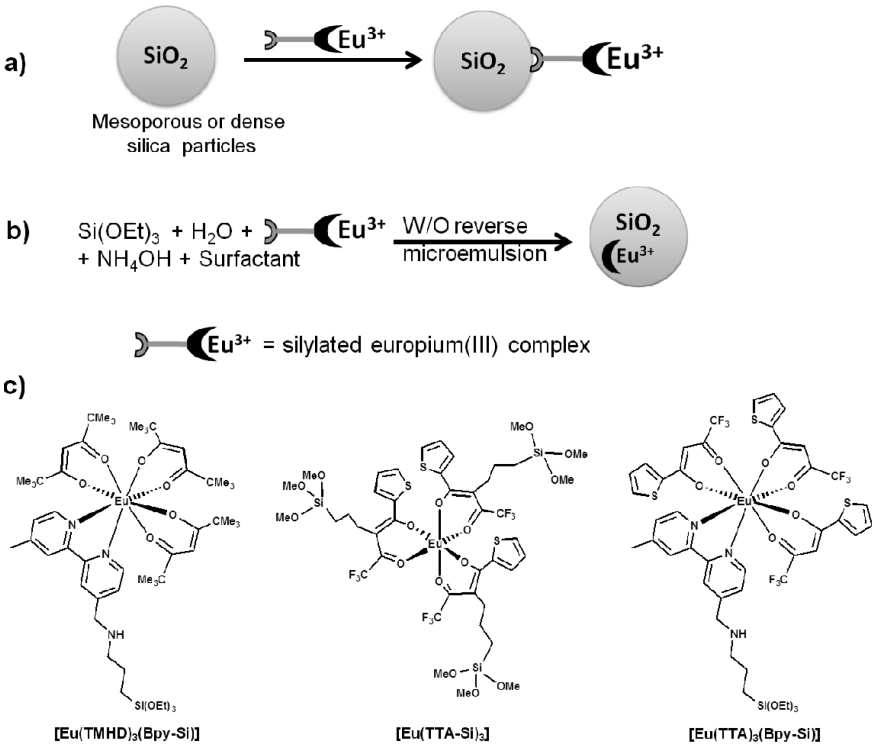

[a](a) Grafting of the silylated Eu^{3+} complex at the surface of mesoporous or dense silica particles. (b) Incorporation of a silylated Eu^{3+} complex in a Stöber-type reaction using a W/O reverse microemulsion system. (c) Silylated europium complexes: $[Eu(TMHD)_3(Bpy\text{-}Si)]$,[21] $[Eu(TTA\text{-}Si)_3]$,[19] and new complex $[Eu(TTA)_3(Bpy\text{-}Si)]$.

the highly specific and sensitive imaging of an environmental pathogen (i.e., *Giardia lamblia*[10]) and to mark cancerous cells.[11] Trivalent europium, in addition, is a structural probe: because of its electronic levels scheme, it is possible to get valuable informations about the local structure of any material from the correct analysis of Eu^{3+} luminescence data. This is one of the goals of this article, which describes the syntheses of new complex $[Eu(TTA)_3(Bpy\text{-}Si)]$ and its related silica-based hybrids together with the investigation of their photoluminescence propeties. As a proof of the potential of the new highly luminescent hybrid NPs, two examples of luminescence imaging appropriated to the study of planctonic or colonized bacteria are given.

The first example is the exploration of *Pseudomonas aeruginosa* (*P. aeruginosa*) biofilms by confocal laser scanning microscopy (CLSM). Biofilm is the normal lifestyle of bacteria, consisting of microorganisms generally entrapped in a self-produced matrix of extracellular polymeric substances (EPS) attached to a solid surface.[12] The control of biofilms is a public health and economic issue. Biofilm formation is a widespread phenomenon in the industrial, medical, and environmental fields. In the medical field, biofilms are involved in nosocomial infections as a result of the contamination of medical devices.[13] Biofilms are known to be much more resistant than planktonic bacteria to antibiotics and biocides, thus demanding their exploration. Luminescent latex-based particles coupled to CLSM have revealed heterogeneities of the diffusion[14,15] and the spatial distribution[16] of particles inside biofilms. New kinds of luminescent nanoparticles incorporating a ruthenium(II) complex into silica have recently been prepared[17] and fruitfully employed for the exploration of biofilms. The possibility to expand the choice of luminescent nanoprobes for biofilm exploration by employing a new europium complex covalently bonded to silica nanoparticles is investigated here.

The second example reported is the labeling and fluorescent imaging of *Escherichia coli (E. coli)*. *E. coli* bacteria are the basis of several human diseases, with the contamination originating mainly from the feces of warm-blooded animals. In this way, quick methodologies for detection and imaging are required to control the contamination of water, food, and hospital equipment. Qin et al.[18] have proposed a specific routine for *E. coli* DNA detection using a Eu^{3+} β-diketone complex incorporated into silica nanoparticles linking an IgG antibody. This bioassay was based on the time-gated detection of the europium luminescence and has shown satisfactory stability, sensitivity, and selectivity. However, developing any detection of *E. coli* by luminescence imaging, without previous preparation steps such as DNA extraction, would be very valuable. The selectivity of the labeling requires the conjugation of a specific antibody to the luminescent nanoparticle. It will be shown hereafter that a silylated europium complex grafted on silica nanoparticles is an appropriate light emitter, after being functionalized with a specific monoclonal antibody, for the fast detection of selectively labeled *E. coli* bacteria.

The original route involving the covalent grafting of luminescent Eu(III) complexes onto silica substrates first requires the design of organosilylated europium complexes combining an efficient antenna effect and alkoxysilane moiety to ensure covalent grafting on any silica substrate (Scheme 1a). One can therefore design the substrate with any morphology,

size, and other adjusted characteristics. Also, the silylated complexes can be incorporated into silica nanoparticles (Scheme 1b), taking advantage of the strong covalent siloxane bonds that are created, which prevents any release of the luminescent complex.

In our previous work, the TTA-Si ligand, based on TTA = 2-thenoyl-trifluoroacetone, known as one of the most efficient sensitizers of Eu^{3+} emission, has been designed, and the related red emitting $[Eu(TTA\text{-}Si)_3]$ complex has been grafted onto or incorporated into silica particles.[19] Alternatively, the silylating group can be supplied by a bipyridine moiety[20] as demonstrated with $[Eu(TMHD)_3(Bpy\text{-}Si)]$ with Bpy-Si equal to $Bpy\text{-}CH_2NH(CH_2)_3Si(OEt)_3$.[21] We present here the synthesis of bifunctionnal complex $[Eu(TTA)_3(Bpy\text{-}Si)]$ (Scheme 1c), combining the antenna TTA and the organosilane Bpy-Si. Luminescent silicated particles have been engineered by the two routes described in Scheme 1a,b. The grafting procedure has been performed on dense silica nanoparticles or mesoporous silica microparticles. The incorporation of new complex $[Eu(TTA)_3(Bpy\text{-}Si)]$ into silica nanoparticles by the so-called Stöber methodology has also been successfully achieved. Luminescence properties of the hybrid particles are examined, compared to those of the corresponding hybrids containing $[Eu(TTA\text{-}Si)_3]$ in our previous work,[19] and discussed with respect to their potential use as luminescent labels.

2-. EXPERIMENTAL SECTION

2.1. Materials. All reagents were purchased from Acros, Aldrich, SDS, New Biochem, Fluka, or Quimis and were used as received. $[Eu(TTA)_3(H_2O)_2]$ and $[Gd(TTA)_3(H_2O)_2]$ complexes were obtained by the methodology described by Fernandes and Melbe.[22,23] The Bpy-Si ligand was synthetized as described in previous work.[20] The dense silica support chosen was the Ludox AS40 aqueous sol (Aldrich), 40 wt % SiO_2, average particle size 24 nm ± 2 nm, and 138 $m^2\ g^{-1}$ specific surface area by BET. Spherical mesoporous SiO_2 particles were obtained by the spray pyrolysis methodology as described in previous work[24] by using cetyltrimethylammonium bromide (CTAB) as the structure-directing agent. Mesoporous particles with a wide dispersion of sizes (average size of 600 ± 300 nm) and a specific surface area value (BET) of 940 $m^2\ g^{-1}$ were obtained. Chloroform, tetrahydrofuran, dichloromethane, methanol, diethylether, and ethanol were purified by distillation in an inert atmosphere before use. The Schlenk system was used for all manipulations concerning the preparation of the ligand and/or the complex to prevent the hydrolysis reaction of the alkoxy functional groups. Ultrapure water (resistivity 18.2 MΩ cm^{-1}) was obtained from a Millipore Milli-Q water purification system. *E. coli* strain ATCC 25922 and *Pseudomonas aeruginosa* PAO1 were used for biological applications.

2.2. Characterization Methods. FTIR and DRIFT spectra were obtained in the spectral range from 4000 to 400 cm^{-1} with a Bruker Vector 22 (KBr dispersion) or a Perkin-Elmer 1760 (DRIFT, DTGS detector) spectrometer. Mass spectra were recorded by FAB using a Nermag R10-10 spectrometer or a TSQ 7000 Thermo-Quest spectrometer. UV−vis spectra were recorded using a Varian UV−visible Cary 1E spectrometer in the range of 900−200 nm. C, H, and N elemental analyses were performed on a Carlo Erba instrument (EA 1110). Nitrogen content allows the determination of the grafting or incorporation ratio, *R*, expressed in millimoles of complex per gram of silica. Luminescence spectra were recorded at room temperature using a Jobin-Yvon model Fluorolog FL3-22 spectrometer equipped with a R928 Hamamatsu photomultiplier and a 450 W Xe excitation lamp. Excitation spectra were corrected with respect to the Xe lamp intensity and the spectrometer (excitation monochromator) response, and emission spectra were corrected for the spectrometer (emission monochromator) response. Measurements of emission decay were performed with the same equipment by using a pulsed Xe (3 μs bandwidth) source. The particle shape and size were examined by TEM using a Philips model CM20 FEG microscope. Luminescence images were obtained with a fluorescence microscope (Leica DMRXE) with DFC300F Xn using a Leica Image Manager 50 software camera. The excitation was performed at 365 ± 5 nm, and the luminescence was recorded over the entire visible spectrum from 400 to 800 nm. The CLSM was performed with a Leica SP2 confocal laser scanning system equipped with an upright microscope and a different laser source (diode laser at 405 nm or argon laser at 488 nm).

2.3. Synthesis. *2.3.1. [Eu(TTA)$_3$(Bpy-Si)] and [Gd(TTA)$_3$(Bpy-Si)] Complexes.* Bpy-Si (0.5 mmol, 202 mg) and $[Eu(TTA)_3(H_2O)_2]$ (0.5 mmol, 428 mg) or $[Gd(TTA)_3(H_2O)_2]$ (0.5 mmol, 410 mg) were added to 20 mL of anhydrous tetrahydrofuran. The reaction mixture was kept under a nitrogen atmosphere and stirred for 3 h. The solvent was evaporated, and the resulting powder was washed with pentane and diethyl ether and dried under vacuum.

2.3.1.1. [Eu(TTA)$_3$(Bpy-Si)]. ($EuC_{45}H_{45}N_3F_9O_9S_3Si$, MW 1215.05 g mol^{-1}): yellow powder, yield 62%. Elemental analysis found (calcd)%: C, 44.29 (44.48); H, 3.62 (3.40); N, 3.44 (3.46)%. Mass spectrum (FAB): 1109 $[M\text{-}(CH_2)_3Si(OC_2H_5)_3]$, 996 [M-TTA]. UV (acetonitrile, 2.5×10^{-5} mol L^{-1}): 240 nm (ε = 23 650 L mol^{-1} cm^{-1}), 269 nm (ε = 30 400 L mol^{-1} cm^{-1}), 281 nm (ε = 27 150 L mol^{-1} cm^{-1}), and 338 nm (ε = 54 350 L mol^{-1} cm^{-1}).

2.3.1.2. [Gd(TTA)$_3$(Bpy-Si)]. ($GdC_{45}H_{45}N_3F_9O_9S_3Si$, MW 1227.4 g mol^{-1}): yellow powder, yield 69%. Elemental analysis found (calcd)%: C, 43.90 (44.14); H, 3.25 (3.70); N, 3.69 (3.43)%. Mass spectrum (FAB): *m/z* 1228 $[M + H]^+$.

2.3.2. Luminescent Hybrids. Two different procedures were used: (1) the complex was grafted onto the particle surface (Ludox AS40 and mesoporous silica) and (2) the complex was incorporated during the silica particle preparation by a modified Stöber synthesis using water-in-oil (W/O) reverse microemulsion methodology.[19] The different hybrids were noted as SiO_2*meso*-$[Eu(TTA)_3(Bpy\text{-}Si)]$, SiO_2-$[Eu(TTA)_3(Bpy\text{-}Si)]$, and SiO_2@$[Eu(TTA)_3(Bpy\text{-}Si)]$ (i.e., mesoporous silica, Ludox AS40, and the incorporating process, respectively). Both types of hybrids are chemically stable for months.

2.3.2.1. SiO$_2$meso-[Eu(TTA)$_3$(Bpy-Si)] and SiO$_2$-[Eu(TTA)$_3$(Bpy-Si)]. Ludox silica sol (500 mg) or mesoporous silica (200 mg) was suspended in ethanol (10 mL) and reacted with 0.16 mmol (200 mg) of $[Eu(TTA)_3(Bpy\text{-}Si)]$. The mixtures were stirred for 72 h at 295 K in an air atmosphere. The resulting suspensions were dialyzed for 72 h, and the solids were isolated by centrifugation at 15 000 rpm for 15 min. The obtained solids were washed with ethanol, dichloromethane, and diethyl ether and then dried under vacuum for 2 h.

SiO_2-$[Eu(TTA)_3(Bpy\text{-}Si)]$: Elemental analysis %, found (calcd), *R* = 0.30 mmol g^{-1}: C, 16.36 (16.20); H, 2.46 (1.23); N, 1.26 (1.26).

SiO_2*meso*-$[Eu(TTA)_3(Bpy\text{-}Si)]$: Elemental analysis %, found (calcd), *R* = 0.64 mmol g^{-1}: C, 32.95 (34.45); H, 3.07 (2.61); N, 2.68 (2.68).

2.3.2.2. SiO$_2$@[Eu(TTA)$_3$(Bpy-Si)]. A solution of 0.016 mmol (20 mg) of $[Eu(TTA)_3(Bpy\text{-}Si)]$ in 2 mL of octanol was added to a W/O microemulsion that was prepared by mixing 4.6 mL of TritonX-100, 20 mL of cyclohexane, and 3 mL of *n*-octanol. Afterward, 266 μL of TEOS and 160 μL of NH_4OH were added. The reaction was stirred for 24 h followed by the addition of acetone in order to break the microemulsion and recover the particles. The particles were washed with water, ethanol, and diethyl ether and then dried in vacuum for 2 h.

SiO_2@$[Eu(TTA)_3(Bpy\text{-}Si)]$: Elemental analysis found (calcd): *R* = 0.31 mmol g^{-1}: C, 15.98 (16.69); H, 2.48 (1.27); N, 1.30 (1.30).

2.4. *P. aeruginosa* PAO1 Biofilm. Biofilms were grown as previously described by Khalilzadeh et al.[25] at 37 °C in 6-well microplates containing modified broth biofilm (MBB) (6 mL). After initial inoculation with a 10^3 CFU mL^{-1} bacteria suspension of PAO1, the medium MBB was renewed at 2, 4, 6, 20, 24, and 48 h after two gentle rinses with sterilized distilled water (6 mL). Biofilms were grown for 3 days. After the period of growth, the wells were emptied and 6 mL of an aqueous suspension of SiO_2-$[Eu(TTA)_3(Bpy\text{-}Si)]$ at 0.05 mg mL^{-1} was introduced. Beforehand, the aqueous suspension

was filtered through Millipore membranes (0.2 μm pore size) in order to sterilize and filter out large aggregates of nanohybrids. Incubation was performed 16 h before confocal microscopy observations in order to allow nanohybrids to diffuse through biofilms. Before the CLSM observation, the biofilms were rinsed to remove excess hybrids that did not penetrate the sample. All of the experiments were carried out at room temperature. To observe biofilms directly, a water-immersion objective was used (63 × 0.9 N.A). Image stacks were recorded in the z direction with a 0.3 μm increment between two focal planes. Bacteria were labeled with a DNA stain, SYTO9 (Molecular Probe, Invitrogen, France). SYTO9 (0.5 μL, 5 mM in DMSO) was added to the wells. SYTO9 was excited with an argon laser (laser power 25%, λ_{exc} = 488 nm), and the fluorescence was collected with a spectral bandwidth of 498−533 nm. Finally, SiO_2-[Eu(TTA)$_3$(Bpy-Si)] was excited with a diode laser (laser power 10 mW, used at 20% power, λ_{exc} = 405 nm), and the fluorescence was collected with a spectral bandwidth of 580−630 nm. Recorded images were processed with Image J version 1.42i (http://rsbweb.nih.gov/ij/index.html). Three-dimensional representations were reconstituted with the Volume viewer plug-in.

2.5. Functionalization of Nanohybrids and Labeling of *E. coli*. *2.5.1. Addition of Blocked Amino Acid at the Nanohybrid Surface, SiO_2-[Eu(TTA)$_3$(Bpy-Si)]-NH_2Fmoc.* Fmoc-ε-Ahx-OH (Biochem New, 0.6 mmol, 0.214 g) in 10.0 mL of dichloromethane was cooled to 0 °C. In the reaction system, 0.30 mmol (48 μL) of *N*,*N*′-diisopropylcarbodiimide was added, and the mixture was stirred for 30 min. Then the solvent was evaporated and the obtained anhydride was redissolved in 2 mL of dimethylformamide. This solution was transferred over 160 mg of particles previously dispersed in DMF; at that time, the catalyst (4-dimethylamino-pyridine, 0.96 mol, 8 mg) was added. The mixture was stirred for 24 h. Then the functionalized particles were separated by centrifugation and extensively washed first with DMF and then with Milli-Q water and lyophilized for 12 h.

SiO_2-[Eu(TTA)$_3$(Bpy-Si)]-NH_2Fmoc: R = 0.31 mmol g^{-1} SiO_2

2.5.2. Immobilization of the IgG1 Antibody on SiO_2-[Eu(TTA)$_3$(Bpy-Si)]-NH_2Fmoc. (i) Take off the Fmoc group. Previously prepared (SiO_2: [Eu]-NH_2Fmoc) particles (100 mg) were redispersed in 5.0 mL of piperidine solution (20% v/v in DMF) under stirring for 30 min, followed by centrifugation and washing (with DMF, five times), which is mandatory for removing the Fmoc protecting group.

(ii) Insert the linkage agent (protein A). In the first step, 70 mg of the Fmoc-less obtained particles were redispersed in 5.0 mL of DMF under stirring, and 1.2 mg of glutaric anhydride was added. The reaction was carried out in 24 h, and the excess glutaric anhydride was removed by washing with DMF and centrifugation (five times). Then the solids were dried at room temperature under reduced pressure. In the second step, 65 mg of the glutaric hybrid was dispersed in 2.5 mL of phosphate saline buffer (PBS, pH 7.0) under stirring. Five milligrams of EDC [*N*-ethyl-*N*-(3-dimethylaminopropyl)-carbodiimide] was added as the catalyst for the reaction between the carboxylic groups from the glutaric system and protein A. Finally, under mild stirring, an excess of protein A (125 mg dispersed in 1 mL of PBS, pH 7.0) was added. The reaction was continued for 2 h and 30 min, followed by centrifugation and rinsing with H_2O (three times) and dried under vacuum for 12 h at 25 °C.

(iii) IgG1 antibody coupling. SiO_2-[Eu(TTA)$_3$(Bpy-Si)]-NH_2-protein A hybrids (50 mg) were redispersed in 4 mL of phosphate saline solution (PBS, pH 7.0) that was slowly stirred. Then, 0.37 mg of IgG1 monoclonal antibody (dispersed in 1 mL of PBS, pH 7.0) was added. The incubation process was carried out for 4 h, followed by centrifugation and washing with H_2O (two times). The final product, SiO_2-[Eu(TTA)$_3$(Bpy-Si)]-IgG1, was redispersed in PBS buffer (pH 7.0) and stored at −20 °C.

2.5.3. Luminescence Imaging of E. coli Bacteria. *E. coli* labeling was carried out by fluorescence microscopy. An *E. coli* culture was grown into BHI agar microbiological cultures (brain heart infusion, Sigma-Aldrich); an aliquot was redispersed in BHI liquid and kept for growth in the microbiological cultures. The bacteria sample was prepared on the microscope slide; the bacterial culture was dried at room temperature, and *E. coli* immobilization was assured by a flame process. The suspension of particles in RPMI-1640 (Roswell Park Memorial Institute, Sigma-Aldrich) solution was dropped onto the culture. The mixture of bacteria and particles was incubated for 30 min at room temperature. Finally, the slides were washed three times with the RPMI-1640 solution, dried at room temperature, and analyzed by fluorescence microscopy.

3. RESULTS AND DISCUSSION

3.1. Characterization of the [Eu(TTA)$_3$(Bpy-Si)] Complex and Silica-Based Hybrids. Bipyridine silylated ligand Bpy-Si was synthesized as described by Cousine et al.,[20] and the synthesis of [Eu(TTA)$_3$(Bpy-Si)] was based on the methodology established[21] where 1 equiv of [Eu(TTA)$_3$(H$_2$O)$_2$] was reacted with 1 equiv of Bpy-Si at room temperature in 62% yield. Analysis by infrared spectroscopy shows the characteristic bands of the TTA binder, for example, the stretching vibration at 1627 υ_s(C═O) and bands at 1578, 1520, and 1407 υ(C═C, C═S) assigned to the plane thenoyl ring. The vibrations of the silylated dipyridine ligand are observed at 3431 υ_{as}(NH), 1578 υ(C═C, C═N ring), 1222 υ(Si−C), 1089 υ(Si−O−C), 962 δ(Si−O), and 790 δ(C−H$_{ar}$). The elemental analysis agrees with the proposed formula $EuC_{45}H_{45}N_3F_9O_9S_3Si$, which is confirmed by mass spectroscopy with the presence of fragment [M−TTA]$^+$ at m/z = 996. Furthermore, the isotopic pattern is in agreement with the stoichiometry proposed in Scheme 1c.

The grafting of the silylated europium complex is a smart strategy for bringing about intense red luminescence in silica-based nanoparticles without the risk of leaching during the elaboration or during any further use in solution. Silylated europium complex [Eu(TTA)$_3$(Bpy-Si)] has been successively grafted onto the surface of dense silica nanoparticles and mesoporous silica microparticles following Scheme 1a and incorporated into the bulk of silica nanoparticles following Scheme 1b.

Grafting was undertaken by the reaction of excess complex with the silica at room temperature in dry ethanol. Two kinds of silica particles have been considered for grafting: mesoporous microparticles from spray pyrolysis[24] and commercial dense nanoparticles Ludox AS40. Pyrolysis provides a material with a high degree of organization of the pores without organic residues that is fully capable of further functionalization of the surface. The Ludox AS40 nanoparticles are monodisperse particles (at pH 9) and have numerous surface silanols free for grafting to alkoxysilanes. When the mesoporous silica matrix was used as the starting silica, substrate activation by heating under vacuum ascertained the absence of physisorbed molecules such as water or any residual structure-directing agent, whereas for the grafting of [Eu(TTA)$_3$(Bpy-Si)] on Ludox silica the presence of water could not be prevented. In both cases, silica-grafted particles were purified by dialysis and further washing and centrifugation.

The [Eu(TTA)$_3$(Bpy-Si)] complex was incorporated into silica nanoparticles using octanol as a cosurfactant and a molar ratio of cosurfactant to surfactant equal to 4.1. Under these conditions, spherical silica nanoparticles that are uniform in size and incorporate new complex SiO_2@[Eu(TTA)$_3$(Bpy-Si)] have been isolated.

DRIFT spectra show the signature of the silylated europium complex in each silica material with the presence of the stretching vibration of the ketone group at 1629 or 1640 cm^{-1} together with a narrow band at 1414 cm^{-1} for the thenoyl moiety. The stretching vibration υ(Si−C) of the complex overlaid with the characteristics of the siloxane bulk υ(Si−O) involves a slight shift and increase in the maxima at 1240 cm^{-1}.

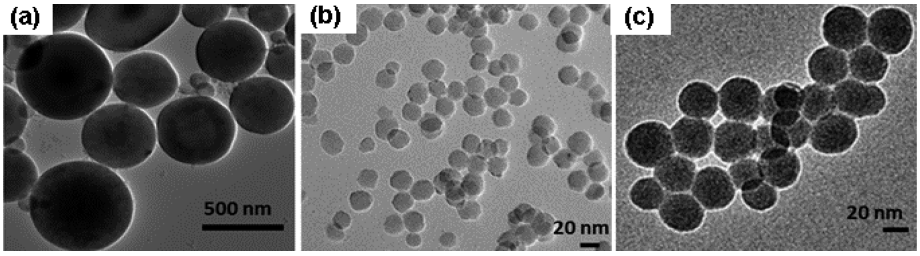

Figure 1. TEM images of the different hybrids: (a) SiO_2*meso*-[$Eu(TTA)_3$(Bpy-Si)], (b) SiO_2-[$Eu(TTA)_3$(Bpy-Si)], and (c) SiO_2@[$Eu(TTA)_3$(Bpy-Si)].

Moreover, the spectra of incorporated nanohybrid SiO_2@[$Eu(TTA)_3$(Bpy-Si)] and grafted SiO_2-[$Eu(TTA)_3$(Bpy-Si)] exhibit weak bands at 2980 and 2878 cm^{-1} corresponding to asymmetric and symmetric stretching vibrations of alkyl groups, respectively.

Figure 1 shows TEM images obtained for the three silica-based materials (a) SiO_2*meso*-[$Eu(TTA)_3$(Bpy-Si)], (b) SiO_2-[$Eu(TTA)_3$(Bpy-Si)], and (c) SiO_2@[$Eu(TTA)_3$(Bpy-Si). The mesoporous silica obtained by spray pyrolysis is made of spherical submicrometer particles with a relatively important size dispersion. A characteristic image of the grafted particles SiO_2*meso*-[$Eu(TTA)_3$(Bpy-Si)] is given Figure 1a. The mesochannels in each sphere form very well ordered hexagonal arrays with a pore diameter of about 2 nm (Supporting Information, Figure S1). The interest in such silica particles is in their large surface area (940 m^2 g^{-1}) that promotes a high level of grafting and a pore diameter allowing free diffusion inside them. As expected, the SiO_2-[$Eu(TTA)_3$(Bpy-Si)] particles appear with a uniform size (28 ± 2 nm) that is slightly increased from the size of the starting particles (24 ± 2 nm) in Figure 1b. Dense silica particles SiO_2@[$Eu(TTA)_3$(Bpy-Si)] obtained by the modified Stöber reaction are spherical and also uniform in size at 45 ± 5 nm (Figure 1c). Because the silylated europium complex was hydrolyzed and aggregated in the water pool in the microemulsion, the europium complex is expected to be evenly distributed throughout the silica network.

Table 1 gives grafting and incorporation ratios, *R*, expressed in millimoles of complex per gram of silica. These values were

Table 1. Size Distribution and Complex [$Eu(TTA)_3$(Bpy-Si)], noted as [Eu], and Grafting or Incorporation Ratios (*R*) for the Three Types of Hybrids[a]

hybrids	average size diameter, nm	*R*, mmol [Eu] g^{-1} SiO_2	$N_{[Eu]}$, nm^{-2}	$N_{[Eu]}$ $particle^{-1}$
SiO_2*meso*-[$Eu(TTA)_3$(Bpy-Si)]	600 ± 300	0.64	0.5	
SiO_2-[$Eu(TTA)_3$(Bpy-Si)]	28 ± 2	0.30	1.3	3000
SiO_2@[$Eu(TTA)_3$(Bpy-Si)]	45 ± 5	0.31		18 000

[a] *R* is given in mmols of [Eu] per gram of silica; $N_{[Eu]}$ is the number of complexes per particle.

calculated from elemental analysis based on the nitrogen content. Values are in the range of 0.64 to 0.30 mmol g^{-1}. The grafting ratios observed for the mesoporous material (0.64 mmol g^{-1}) and for Ludox silica (0.30 mmol g^{-1}) are significantly higher than those found for [$Eu(TTA\text{-}Si)_3$][19] (0.41 and 0.21 mmol g^{-1}, respectively) or for [$Eu(TMHD)_3$(Bpy-Si)][21] (0.41 mmol g^{-1}) at Ludox silica particles. The number of grafted complexes per nm^2 can be calculated using the observed grafting ratios and the specific areas of the starting materials. Around 1.3 europium complexes per nm^2 are grafted onto Ludox whereas 0.5 complex per nm^2 is grafted onto the mesoporous material. This difference can be attributed to the different hydroxylation ratios of each silica matrix because the number of free silanol groups available for grafting is smaller for freshly activated mesoporous silica than for the Ludox silica aqueous solution. An important question about the grafted SiO_2-[$Eu(TTA)_3$(Bpy-Si)] nanoparticles is evaluating if there is still some silica surface free for further biofunctionalization. When we take the average size of one complex molecule as 0.25 nm^2,[20] the maximum coverage of one particle with a diameter of 24 nm will be achieved at 7238 complex units [Eu], that is, 0.8 mmol g^{-1} (taking the particle density as 2 g cm^{-3}). With the observed grafting ratio of 0.3 mmol g^{-1} corresponding to 3000 [Eu] per particle, about 60% of the surface is still free for further reaction.

The microemulsion process allows the incorporation of a large amount of [$Eu(TTA)_3$(Bpy-Si)] because according to the nitrogen content a quantity of 0.31 mmol of complex per gram of silica has been calculated, giving 18 000 complex units per nanoparticle. With these numerical values, the concentration in active species [$Eu(TTA)_3$(Bpy-Si)] is 0.63 mmol cm^{-3}. This concentration is relatively high compared to 1.7 mmol cm^{-3} calculated from the crystal structure of the analogous unsilylated complex [$Eu(TTA)_3$(Bpy)][26] (unit cell volume of 3.97 nm^3 with four molecular units). Some other lanthanides complexes have been embedded in silica nanoparticles using W/O microemulsion synthesis. More often the encapsulation starts from unsilylated complexes, and the number of optically active species per particle has not often been reported. This is the case for BPTA-Tb chelates[27] (BPTA = *N*,*N*,*N*′,*N*′-[2,6-bis(3′-aminomethyl-1′-pyrazolyl)-phenylpyridine]tetrakis-(acetate)), with 1500 Tb(BPTA) units per nanoparticle (42 nm), which means 0.06 mmol cm^{-3}. A large helicate bimetallic Eu(III) complex has been encapsulated in 55 nm silica particles at 540 complex units per nanoparticle, meaning 0.01 mmol cm^{-3}.[11] The silylated dual complex Eu/Tb(BBCAP) (BBCAP = 2,9-bis[*N*,*N*-bis(carboxymethyl)aminomethyl]-1,10-phenanthroline) has also been incorporated into silica by W/O, but the grafting ratio is not given.[28] The last example is that of Xu et al.,[29] who performed the covalent bonding between complex Eu(BHHCT) (BHHCT = 4,4bis(1,1,2,2,3,3-heptafluoro-4,6-hexanedion-6-yl)chlorosulfo-oterphenyl) and an aminated silica. Up to five cycles of coupling reaction were necessary to obtain efficient luminescent labels with the high reported value of 6.3×10^5 Eu(BHHCT) per 55 nm nanoparticles, that is, 12 mmol cm^{-3}, which seems to be overestimated.[30]

Table 2. Judd–Ofelt Intensity Parameters (Ω_2, Ω_4), Radiative Rates (A_{rad}), Experimental Lifetimes (τ_{exp}), Nonradiative Rates ($A_{N\text{-}rad}$), and Quantum Efficiencies (q) of the Complexes and Hybrids[a]

complex and hybrids	$\Omega_2 \times 0.10^{-20}$ m^2	$\Omega_4 \times 0.10^{-20}$ cm^2	A_{rad} ms^{-1}	τ_{exp} ms	$A_{N\text{-}rad}$ ms^{-1}	q	ϕ
$[Eu(TTA)_3(H_2O)_2]$[31]	33	4.6	0.79	0.26	3.06	0.21	
$[Eu(TTA\text{-}Si)_3]$[19]	40 ± 2	5.9 ± 0.3	1.15 ± 0.06	0.56 ± 0.06	0.64 ± 0.06	0.64 ± 0.09	
$[Eu(TTA\text{-}Si)_3]$[19] 2.5×10^{-5} mol L^{-1} CH_3CN	31 ± 1	4.2 ± 0.2	0.75 ± 0.04	0.60 ± 0.06	0.92 ± 0.09	0.45 ± 0.05	0.30 ± 0.03
$[Eu(TTA)_3(Bpy\text{-}Si)]$	26 ± 1	5.7 ± 0.3	1.02 ± 0.05	0.60 ± 0.06	0.65 ± 0.06	0.61 ± 0.09	
$[Eu(TTA)_3(Bpy\text{-}Si)]$ 2.5×10^{-5} mol L^{-1} CH_3CN	20 ± 1	4.1 ± 0.2	1.30 ± 0.06	0.51 ± 0.05	0.66 ± 0.07	0.66 ± 0.09	0.53 ± 0.07
SiO_2*meso*-$[Eu(TTA)_3(Bpy\text{-}Si)]$	17.2 ± 0.8	1.6 ± 0.1	0.63 ± 0.03	0.65 ± 0.06	0.91 ± 0.09	0.41 ± 0.06	
SiO_2-$[Eu(TTA)_3(Bpy\text{-}Si)]$	18.3 ± 0.9	1.9 ± 0.1	0.62 ± 0.03	0.66 ± 0.07	0.90 ± 0.09	0.41 ± 0.06	
SiO_2@$[Eu(TTA)_3(Bpy\text{-}Si)]$	9.6 ± 0.4	5.5 ± 0.3	0.48 ± 0.02	0.55 ± 0.05	1.34 ± 0.13	0.26 ± 0.04	

[a]Quantum yields ϕ were measured for the solutions relative to $[Ru(Bpy)_3]^{2+}$ in water (ϕ = 2.8%).

3.2. Luminescence. Optical properties of complex $[Eu(TTA)_3(Bpy\text{-}Si)]$ diluted in acetonitrile were investigated by absorption and photoluminescence. The absorption spectrum is shown in Supporting Information (Figure S2) with those of Bpy-Si and $[Eu(TTA)_3(H_2O)_2]$, allowing the assignment of the two bands with maxima at 281 nm (ε = 27 150 L mol^{-1} cm^{-1}) and 240 nm (ε = 23 650 L mol^{-1} cm^{-1}) to the Bpy-Si ligand and of the two bands at 338 nm (ε = 54 350 L mol^{-1} cm^{-1}) and 269 nm (ε = 30 400 L mol^{-1} cm^{-1}) to absorption by TTA.

Figure S3 (Supporting Information) gathers the excitation and emission spectra recorded for complex $[Eu(TTA)_3(Bpy\text{-}Si)]$ in the solid state and its solution in acetonitrile. The broad excitation band recorded for the complex in solution essentially reproduces its absorption spectrum. The bands centered at 350 nm, being assigned to the singlet-to-singlet transition in the TTA ligand, has a maximum at 340 nm and a shoulder at 360 nm. The absorption band at 300 nm, which is not observed for the $[Eu(TTA\text{-}Si)_3]$ complex, is probably due to the Bpy-Si ligand being red-shifted with respect to the absorption band (281 nm).

To characterize the ligand triplet state in $[Eu(TTA)_3(Bpy\text{-}Si)]$, the analogous complex of Gd(III) has been synthetized and its photoluminescence has been investigated at liquid nitrogen temperature (Figure S4 in the Supporting Information). The emission of the triplet to ground-state transition is observed at 500 nm, fixing the triplet state at around 20 000 cm^{-1}. The energy of the triplet state is higher than that of the Eu(III) $^5D_0$ state so that energy transfer from the triplet state to $^5D_0$ is favorable whereas back transfer would be much less probable. It may be noticed here that the triplet state in $[Eu(TTA)_3(Bpy\text{-}Si)]$ is localized at a lower energy than the triplet state in $[Eu(TTA\text{-}Si)_3]$, which shows the effect of the additional Bpy-Si ligand on the molecular levels centered on the TTA molecules.

The emission spectra of $[Eu(TTA)_3(Bpy\text{-}Si)]$ in the solid state and diluted in acetonitrile are substantially the same, thereby confirming that the Eu(III) environment is the same in both states (Figure S3 in the Supporting Information). The comparison of Eu^{3+} luminescence data in different hosts may be performed more accurately by the calculation of a set of values: the Judd–Ofelt parameters (Ω_2, Ω_4), the radiative rates (A_{rad}), the experimental lifetimes (τ_{exp}), the nonradiative rates ($A_{N\text{-}rad}$), and the quantum efficiencies (q). The ratios of integrated intensities $I(^5D_0 \rightarrow {}^7F_{J=0,2-6})$ to $I(^5D_0 \rightarrow {}^7F_1)$ may be employed to calculate the $^5D_0 \rightarrow {}^7F_J$ radiative rates $A_{0\text{-}J}$. The $^5D_0 \rightarrow {}^7F_1$ transition is purely magnetically dipolar, and its radiative rate does not depend on the local field imposed by the environment. The $^5D_0 \rightarrow {}^7F_1$ oscillator strength has been calculated from theory, giving $A_{0-1} = 14.65n^3$ in s^{-1}, with n being the medium's refractive index. The values of A_{0-2} and A_{0-4} are related directly to the Judd–Ofelt intensity parameters Ω_2 and Ω_4, respectively, following expressions given in Carlos et al.[7] and Binnemans.[8] Here, as in our previous work,[19] it has been assumed that n = 1.5 and that $^5D_0 \rightarrow {}^7F_{5,6}$ have negligible intensities. The $^5D_0$ radiative rates $A_{rad} = \Sigma(A_{0-J})$ have been calculated and employed to evaluate the $^5D_0$ quantum efficiencies q ($q = \tau_{exp}A_{rad}$). The experimental lifetimes were obtained by fitting the $^5D_0$ luminescence decay with $I = I_0 \exp(-t/\tau_{exp})$ (Figure S5 in Supporting Information). Table 2 gathers the values established for the complex in the solid state, its solution in acetonitrile, and the hybrids and data of interest extracted from the literature.

From these experimental data, the $^5D_0$ quantum efficiencies are 61 and 66% for the $[Eu(TTA)_3(Bpy\text{-}Si)]$ solid complex and its solution, respectively, to be compared with 64 and 45% for $[Eu(TTA\text{-}Si)_3]$. This result supports the fact that the coordination sphere of Eu(III), with the three diketonate groups and the two nitrogen atoms from Bpy-Si, is complete and retained in solution whereas at least two coordination sites are free for interaction with solvent molecules in $[Eu(TTA\text{-}Si)_3]$.

The quantum yield (ϕ), the ratio of emitted to absorbed photons, has been measured for the solution relative to $[Ru(Bpy)_3]^{2+}$.[19,32] For $[Eu(TTA)_3(Bpy\text{-}Si)]$, ϕ is equal to 53%, which is higher than that for $[Eu(TTA\text{-}Si)_3]$ (ϕ = 30%). The ratio of ϕ (the quantum yield for excitation in the ligand) to q (the quantum efficiency of the $^5D_0$ emitting level) expresses the efficiency of the ligand to Eu(III) energy transfer (the sensitization efficiency: $A_{ligand-metal}$): it equals 80% in $[Eu(TTA)_3(Bpy\text{-}Si)]$ versus 67% in $[Eu(TTA\text{-}Si)_3]$, measured under the same excitation conditions. It has been highlighted here that the TTA triplet state is lowered by the Bpy-Si additional ligand, which apparently increases the probability of the TTA to Eu(III) energy transfer. All of these observations highlight the interest in combining Bpy-Si and TTA ligands with the Eu center.

Figure 2 shows excitation and emission luminescence spectra obtained for each hybrid and also those of the $[Eu(TTA)_3(Bpy\text{-}Si)]$ free complex. No noticeable photodegradation was observed during luminescence experiments. Concerning excitation, the same bands already seen for the pure complex are observed for the hybrid systems (Figure 2I). The ligand to europium antenna effect is observed below 450 nm as broad near-UV bands, with the Eu^{3+} 4f–4f transitions being very weak in the visible region. Excitation spectra recorded on powdered materials are more often distorted in the region of high

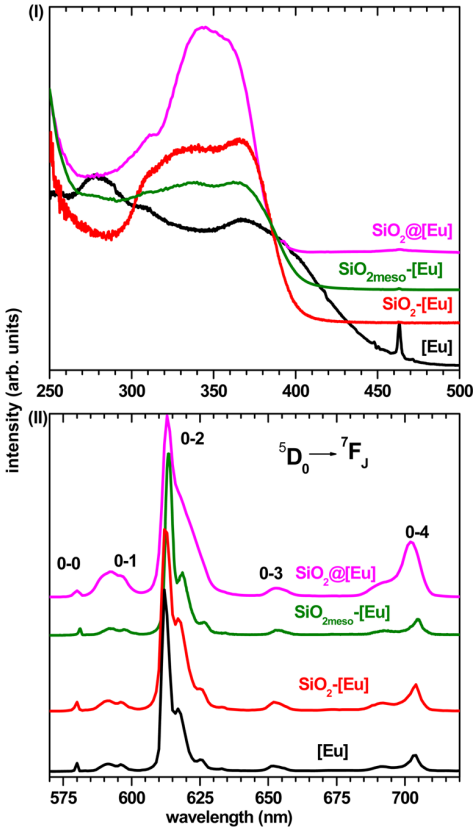

Figure 2. Luminescence results for modified silica particles. (I) Excitation spectra (λ_{em} at 611 nm) and (II) emission spectra (λ_{exc} at 365 nm) for the different solid samples at 298 K. Each spectrum has been normalized and shifted on the *y* axis for clarity and [Eu] = [Eu(TTA)$_3$(Bpy-Si].

absorption, and a similar effect encountered in concentrated solutions has been explained.[33] For the hybrids, because the luminescent species are diluted in silica, distortions are much weaker so that the shape of the excitation band around 350 nm is more similar to that observed for the dilute solution.

The emission spectra recorded for the two grafted hybrids, SiO$_2$-[Eu(TTA)$_3$(Bpy-Si)] and SiO$_2$*meso*-[Eu(TTA)$_3$(Bpy-Si)], are rather similar, which is traduced by similar values of their respective Ω_2, Ω_4, and A_{rad}. The incorporated nanohybrid, SiO$_2$@[Eu(TTA)$_3$(Bpy-Si)], displays broadened emission lines. The overall shape differs more from that of the two other hybrids and from that of the neat complex, reflected by significant differences in the calculated Ω_2, Ω_4, and A_{rad}.

The nonradiative decay rate in the complex, $A_{N\text{-}rad} = (1/\tau_{exp}) - A_{rad} = 0.65$ ms^{-1} (Table 2) is essentially due to coupling with vibrations in the organic ligands. With respect to the pure complex, additional nonradiative de-excitation pathways in the hybrids, with rates of 0.26 to 0.25 ms^{-1} (grafted) and 0.69 ms^{-1} (incorporated), could be the coupling with high-energy vibrations of nearby hydroxyls or with Si−O vibrations of nearby siloxanes. Weak modifications imposed by the silica network on the [Eu] complex structure could also enhance the nonradiative decay rate.

A high radiative rate, A_{rad}, and a good $^5D_0$ quantum efficiency, *q*, are two characteristics of an efficient light emitter, preferably associated with a high absorption rate and sensitization efficiency. For the solid [Eu(TTA)$_3$(Bpy-Si)], A_{rad} = 1.02 ms^{-1} and *q* = 61%, highlighting excellent properties of the free complex. Both characteristics decrease moderately in the grafted hybrid particles with A_{rad} = 0.63 and 0.62 ms^{-1}, respectively, associated with a high efficiency *q* = 41%, whereas incorporated hybrid nanoparticles display slightly inferior characteristics.

At this point, besides the light-emission properties, other physicochemical characteristics of the hybrids must also be taken into account in view of potential applications in the field of bioimaging. The SiO$_2$*meso*-[Eu(TTA)$_3$(Bpy-Si)] particles have a large size and dispersion, 600 ± 300 nm, which rule them out from being employed in bioimaging. The grafted silica particles, SiO$_2$-[Eu(TTA)$_3$(Bpy-Si)], and the silica particles incorporating complex SiO$_2$@[Eu(TTA)$_3$(Bpy-Si)] are nano-sized and monodisperse, with diameters of 28 ± 2 and 45 ± 5 nm, respectively, so both kinds of nanoparticles (denoted in the following text as grafted-NP and incorporated-NP) are good candidates as efficient red-emitters in bioimaging.

The brightness (*B*) of each nanoparticle may be considered to be an intrinsic quality of emitted light when excited at a given wavelength, and it is related to the number of active species in one nanoparticle, $N_{[Eu]}$, to the absorption coefficient at the excitation wavelength, ε, to the sensitization efficiency when excitation is achieved in the ligand, $A_{ligand-metal}$, and finally to the $^5D_0$ quantum efficiency, *q*: $B \approx N_{[Eu]} q \varepsilon A_{ligand-metal}$. Taking into account the numerical values gathered in Tables 1 and 2, we have $B_{(grafted\ NP)} \approx 1230(\varepsilon A_{ligand-metal})_{grafted}$ and

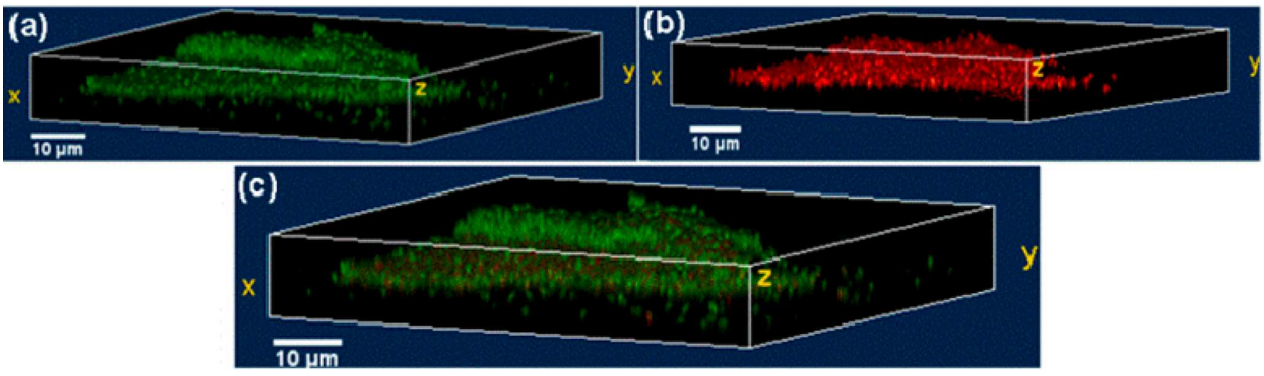

Figure 3. Confocal micrographs treated with ImageJ (35 scans in the *xy* plane) of *P. aeruginosa* biofilms (a) labeled with SYTO 9 (λ_{ex}= 488 nm and λ_{em}= 498−520 nm) and (b) after contact with grafted-NP (λ_{ex}= 405 nm and λ_{em}= 580−630 nm). (c) Merged pictures.

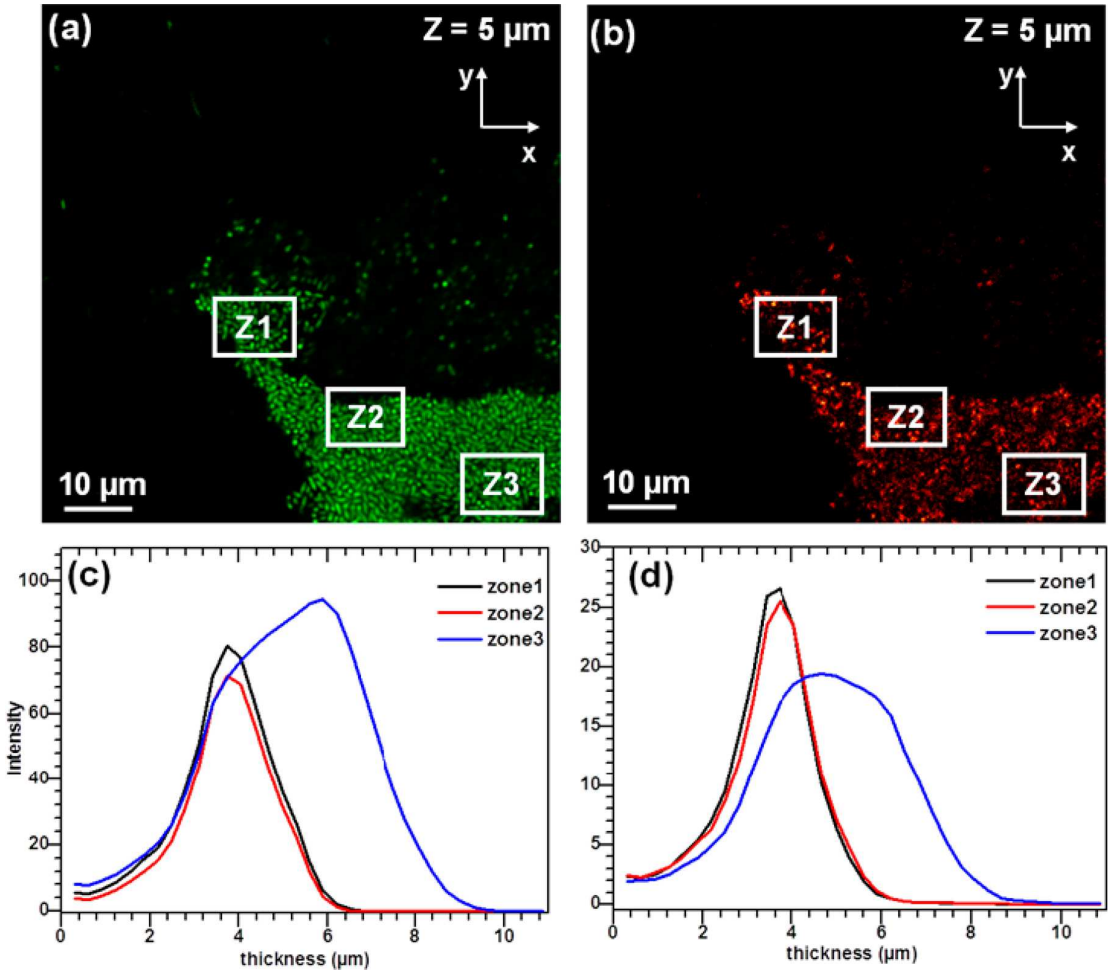

Figure 4. Confocal images at midheight of the *P. aeruginosa* biofilm (a) labeled with SYTO 9 and (b) after contact with grafted-NP. Emission intensity as a function of biofilm thickness for the biofilm (c) labeled with SYTO 9 and (d) after contact with grafted-NP.

$B_{(\text{incorporated NP})} \approx 4680\ (\varepsilon A_{\text{ligand–metal}})_{\text{incorporated}}$. In the following paragraphs, we give experimental evidence that grafted-NP SiO_2-[Eu(TTA)$_3$(Bpy-Si)] are brighter probes, meaning that $(\varepsilon A_{\text{ligand–metal}})$ is higher in grafted systems than in incorporated systems. This can be understood if structural modifications imposed by the silica network on the incorporated complex significantly decrease the ligand to Eu sensitization efficiency.

3.3. Bioimaging Applications. *3.3.1. CLSM Exploration of P. aeruginosa PAO1 Biofilm.* The grafted-NPs were tested as tools for exploring *P. aeruginosa* biofilms using CLSM. In the case of specific biological systems such as biofilms, which are hydrated 3D structures, the advantage of CLSM is the in situ study contrary to the classical electronic microscopies that require dehydrated samples to modify their tridimensional structures. Moreover, CLSM allows in vivo luminescence tracking. Figure 3a shows 3D representations of a *P. aeruginosa* biofilm of 10 μm thickness whose bacteria were labeled with SYTO 9 emitting green luminescence. Figure 3b is the CLSM observation of the same *P. aeruginosa* biofilm after 16 h of contact with grafted-NP dispersed in aqueous suspensions at 0.05 mg mL^{-1}. The red spots correspond to the characteristic emission of the silica hybrids in the range of 580–630 nm. The merged picture, Figure 3c, shows that the red spots of the nanoparticles are evenly distributed within the tridimensional structure of the biofilm.

To ascertain the presence of the grafted-NP inside the 3D biological structure, emission intensities in the snapshot at midheight (z = 5 μm) have been compared, and images are presented in Figure 4a,b. It is clear that the luminescent nanoprobes are inside the biofilm. To evaluate their penetration of the thickness of the biolfilm, we have chosen three regions of interest (ROI), represented by the white squares noted as Z1–3 (Figure 4a,b), and the measurements of the emission intensity have been made from z = 0 to 10 μm. The graph charting the emission intensity as a function of the biofilm thickness is given Figure 4c,d for the bacteria labeled with SYTO9 and grafted-NP, respectively. For the three ROIs, it is obvious that grafted-NP penetrates from the top to the base of the biofilm. This indicates that the small size (28 nm) of grafted-NP is well adapted to the penetration inside the biofilm structure, permitting their free circulation. The surface properties of the particles, that is, their hydrophylicity or hydrophobicity, are also important parameters as has been recently shown with functionalized quantum dots[34] and silicated NP incorporating the ruthenium(II) complex.[17] In the case of grafted-NP, 60% of the outer surface is unmodified silica, so this result proves that the surface of grafted-NP

Scheme 2. Schematic Representation of the IgG1-Functionalized Hybrid Nanoparticles

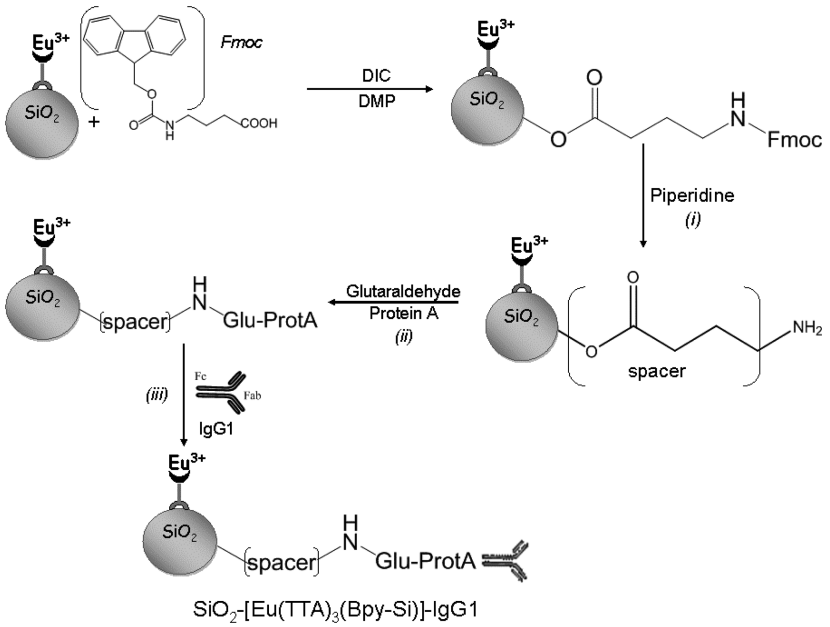

remains hydrophilic enough to allow their diffusion in the entire biofilm. This study validates the use of europium complex [Eu(TTA)$_3$(Bpy-Si)] grafted on silica nanoparticles to explore the *P. aeruginosa* biofilm. Keeping in mind the difficulty of studying such heterogeneous biological systems, these new luminescent NPs are very promising tools. The same experiment was performed with the SiO_2@[Eu(TTA)$_3$(Bpy-Si)] hybrid, but the observed luminescence was too weak, indicating that incorporated-NP was therefore not valuable under the experimental conditions used for CLSM.

3.3.2. Luminescence Imaging of E. coli Bacteria. To test the ability of our luminescent NP in the field of bacterial labeling, further functionalization of the particle surfaces is required. Therefore, a luminescent label was designed, as described in Scheme 2, with three components: a signal-generating unit SiO_2-[Eu(TTA)$_3$(Bpy-Si)], an amino acid spacer, and an anchor group (anti-*E. coli*, IgG1).

The functionalization procedure requires special care, and it was essential to determine the number of reactive groups on the SiO_2 surface available for successive reactions and coupling between the NP and the antibody F_c region. The first functionalization step to bring about the spacer groups was carried out by peptide synthesis on the solid phase,[35] with Fmoc-ε-Ahx-OH. This methodology permits us to determine the number of amino groups available for later reaction, fixing the number of anchor groups admitted to react. After Fmoc deprotection (Scheme 2i), its quantification by UV−vis spectroscopy gives the number of amino groups equal to 0.31 mmols of NH_2 per gram of silica. This value is well adapted to carrying out the functionalization. The next step is the addition of the protein A anchor group (Scheme 2ii). Because the antibody can react with NH_2 groups by both F_c and F_{ab} portions and F_{ab} is specific to *E. coli* bacteria, protein A that binds specifically to the F_c portion of the antibody was used (Scheme 2iii). This immobilization process decreases the random orientation of the antibody molecules on the solid-phase surface,[36] and then the F_{ab} portion of SiO_2-[Eu(TTA)$_3$(Bpy-Si)]-IgG1 is available for highly specific coupling with *E. coli* bacteria.

Bacteria and grafted-NP were incubated for 30 min at room temperature, and then the slides were washed to remove the unbonded particles and analyzed by fluorescence microscopy. The images (Figure 5) display red spots of the Eu^{3+}

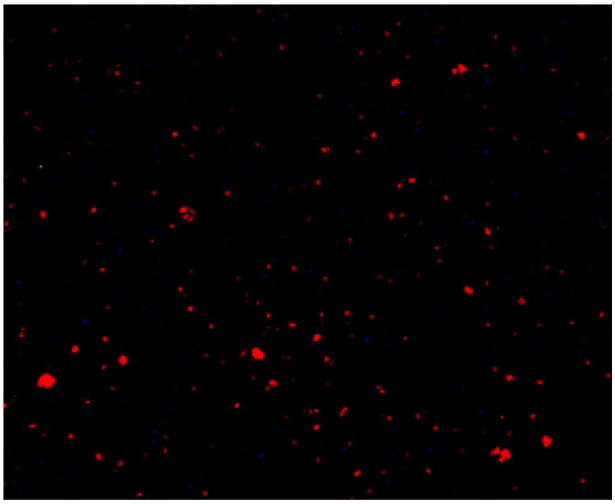

Figure 5. Fluorescence microscopy image of the sample of *E. coli* bacteria labeled with SiO_2-[Eu(TTA)$_3$(Bpy-Si)]-IgG1. The total magnification is 400×.

luminescent labels and confirm that the IgG1 functionalization has permitted the specific bonding of the luminescent label on *E. coli* microorganisms. In a control experiment, the unmodified SiO_2-[Eu(TTA)$_3$(Bpy-Si)] nanoparticles have been tested with same incubation time on the *E. coli* bacteria, but after the washing process, all particles have been removed from the bacterial culture and no emission was detected (Supporting Information Figure S8). The same experiment has been done in

parallel with incorporated-NP, but the Eu^{3+} luminescence was more difficult to detect.

We have demonstrated here that the functionalized hybrid, SiO_2-[Eu(TTA)3(Bpy-Si)]-IgG1, displaying a highly luminescent silica nanoparticle associated at a high affinity and specificity of monoclonal antibodies, provides a new nanosized label adapted to bacterial detection in the immunoassay area.

4. CONCLUSIONS

This work describes an original strategy for designing luminescent silica-based hybrids containing europium chelates. Europium complex $[Eu(TTA)_3(Bpy\text{-}Si)]$ was synthesized and fully characterized by elemental analysis, mass spectrometry, FTIR, and electronic spectroscopy. The europium ion is chelated by three TTA diketonato ligands, known as being among the best organic antennas to sensitize the Eu^{3+} emission. The coordination is completed by bonding a dipyridine moiety of a Bpy-Si silylated ligand. Judd−Ofelt $\Omega_{2,4}$ intensity parameters and radiative and nonradiative decay rates for the Eu^{3+} $^5D_0$ excited state were evaluated. The $^5D_0$ quantum efficiencies (q) of the solid complex and its solution are 61 and 66%, respectively, situating this complex as one of the most highly luminescent europium chelates. The presence of the alkoxysilyl group allows its covalent grafting on any silica surface: it has been completed on two types of silica particles (i.e., mesoporous microparticles and dense nanoparticles). The covalent bonding of $[Eu(TTA)_3(Bpy\text{-}Si)]$ inside the core of uniform silica nanoparticles has also been achieved, requiring a reverse W/O Stöber methodology. The mesoporous particles (600 ± 300 nm) allowed a highly complex grafting ratio and high $^5D_0$ quantum efficiency (41%), and they could be useful substrates for drug delivery, possibly located by luminescence imaging. Two types of silica nanoparticles containing the new complex grafted onto the surface or incorporated into the core were engineered: SiO_2-$[Eu(TTA)_3(Bpy\text{-}Si)]$, with a diameter of 28 ± 2 nm and a high $^5D_0$ quantum efficiency of q = 41%, and SiO_2@$[Eu(TTA)_3(Bpy\text{-}Si)]$, with a diameter of 45 ± 5 nm and q = 26%. These NPs could be used in applications where the stability of silica particles and a high emission intensity are simultaneously required, and their ability has been tested in two types of luminescent bioimaging.

The grafted-NPs have proven to be very promising tools for the exploration of *P. aeruginosa* biofilms by CLSM. Such heterogeneous biological systems are highly involved in nosocomial infections and are extremely difficult to analyze. The possibility to expand the choice of luminescent nanoprobes for biofilm exploration by employing new complex $[Eu(TTA)_3(Bpy\text{-}Si)]$ grafted to silica nanoparticles is demonstrated here. Biofunctionalized luminescent label SiO_2-$[Eu(TTA)_3(Bpy\text{-}Si)]$-IgG1 has been generated, and its specific bonding on *E. coli* bacteria has been tested and imaged by fluorescence microscopy. The strong and durable luminescence of the hybrid NP, associated with the high affinity and specificity of the monoclonal antibody, provides a new type of nanolabel for quick bacterial detection in the immunoassay area.

ASSOCIATED CONTENT

IR data for complexes and DRIFT for hybrids. TEM images of mesoporous silica. Absorption, excitation, and emission spectra for solution and different solid europium complexes. Excitation and emission spectra of a gadolinium analog. $^5D_0$ decay curves. Optical microscopy images of *E. coli*. ATCC25922. Fluorescence microscopy images of grafted-NP and *E. coli*.

AUTHOR INFORMATION

Corresponding Author

*E-mail: menu@chimie.ups-tlse.fr. Tel: 33 5 61 55 84 87. Fax: 33 5 61 55 61 63.

Notes

The authors declare no competing financial interest.

ACKNOWLEDGMENTS

We thank Brazilian agencies FAPESP, CNPq, and CAPES, the CAPES-COFECUB Brazil-France cooperation program for the grant to A.P.D., and L.A. Rocha for profitable discussion with A.P.D.

REFERENCES

(1) Buenzli, J.-C. G.; Piguet, C. Taking advantage of luminescent lanthanide ions. *Chem. Soc. Rev.* **2005**, *34*, 1048−1077.

(2) Buenzli, J.-C. G. Lanthanide luminescence for biomedical analyses and imaging. *Chem. Rev.* **2010**, *110*, 2729−2755.

(3) Bettencourt-Dias, A. Small molecule luminescent lanthanide ion complexes - photophysical characterization and recent developments. *Curr. Org. Chem.* **2007**, *11*, 1460−1480.

(4) Richardson, F. S. Terbium(III) and europium(III) ions as luminescent probes and stains for biomolecular systems. *Chem. Rev.* **1982**, *82*, 541−52.

(5) Escribano, P.; Julian-Lopez, B.; Planelles-Arago, J.; Cordoncillo, E.; Viana, B.; Sanchez, C. Photonic and nanobiophotonic properties of luminescent lanthanide-doped hybrid organic-inorganic materials. *J. Mater. Chem.* **2008**, *18*, 23−40.

(6) Eliseeva, S. V.; Bunzli, J.-C. G. Lanthanide luminescence for functional materials and bio-sciences. *Chem. Soc. Rev.* **2010**, *39*, 189−227.

(7) Carlos, L. D.; Ferreira, R. A. S.; Bermudez, V. D.; Ribeiro, S. J. L. Lanthanide-containing light-emitting organic-inorganic hybrids: a bet on the future. *Adv. Mater.* **2009**, *21*, 509−534.

(8) Binnemans, K. Lanthanide-based luminescent hybrid materials. *Chem. Rev.* **2009**, *109*, 4283−4374.

(9) Wang, L.; Wang, K. M.; Santra, S.; Zhao, X. J.; Hilliard, L. R.; Smith, J. E.; Wu, J. R.; Tan, W. H. Watching silica nanoparticles glow in the biological world. *Anal. Chem.* **2006**, *78*, 646−654.

(10) Wu, J.; Ye, Z.; Wang, G.; Jin, D.; Yuan, J.; Guan, Y.; Piper, J. Visible-light-sensitized highly luminescent europium nanoparticles: preparation and application for time-gated luminescence bioimaging. *J. Mater. Chem.* **2009**, *19*, 1258−1264.

(11) Eliseeva, S. V.; Song, B.; Vandevyver, C. D. B.; Chauvin, A.-S.; Wacker, J. B.; Buenzli, J.-C. G. Increasing the efficiency of lanthanide luminescent bioprobes: bioconjugated silica nanoparticles as markers for cancerous cells. *New J. Chem.* **2010**, *34*, 2915−2921.

(12) Costerton, J. W.; Lewandowski, Z.; Caldwell, D. E.; Korber, D. R.; Lappin-Scott, H. M. Microbial biofilms. *Annu. Rev. Microbiol.* **1995**, *49*, 711−745.

(13) Doggett, R. G.; Harrison, G. M.; Wallis, E. S. Comparison of some properties of pseudomonas aeruginosa isolated from infections in persons with and without cystic fibrosis. *J. Bacteriol.* **1964**, *87*, 427−431.

(14) Guiot, E.; Georges, P.; Brun, A.; Fontaine-Aupart, M. P.; Bellon-Fontaine, M. N.; Briandet, R. Heterogeneity of diffusion inside microbial biofilms determined by fluorescence correlation spectroscopy under two-photon excitation. *Photochem. Photobiol.* **2002**, *75*, 570−578.

(15) Habimana, O.; Steenkeste, K.; Fontaine-Aupart, M.-P.; Bellon-Fontaine, M.-N.; Kulakauskas, S.; Briandet, R. Diffusion of nano-

particles in biofilms is altered by bacterial cell wall hydrophobicity. *Appl. Environ. Microbiol.* **2011**, *77*, 367−368.
(16) Okabe, S.; Yasuda, T.; Watanabe, Y. Uptake and release of inert fluorescence particles by mixed population biofilms. *Biotechnol. Bioeng.* **1997**, *53*, 459−469.
(17) Mauline L. UPS Elaboration de Nanoparticules de Silice Bifonctionnelles. Outils Innovants pour l'Exploration de Biofilms à Pseudomonas Aeruginosa. Ph.D. Thesis, Université de Toulouse, Toulouse, Mars 2012.
(18) Qin, P.-Z.; Niu, C.-G.; Zeng, G.-M.; Ruan, M.; Tang, L.; Gong, J.-L. Time-resolved fluorescence based DNA detection using novel europium ternary complex doped silica nanoparticles. *Talanta* **2009**, *80*, 991−995.
(19) Duarte, A. P.; Gressier, M.; Menu, M.-J.; Dexpert-Ghys, J.; Caiut, J. M. A.; Ribeiro, S. J. L. Structural and luminescence properties of silica-based hybrids containing new silylated-diketonato europium-(III) complex. *J. Phys. Chem. C* **2011**, *116*, 505−515.
(20) Cousinie, S.; Gressier, M.; Alphonse, P.; Menu, M.-J. Silica-based nanohybrids containing dipyridine, urethan, or urea derivatives. *Chem. Mater.* **2007**, *19*, 6492−6503.
(21) Cousinie, S.; Gressier, M.; Reber, C.; Dexpert-Ghys, J.; Menu, M.-J. Europium(III) complexes containing organosilyldipyridine ligands grafted on silica nanoparticles. *Langmuir* **2008**, *24*, 6208−6214.
(22) Melby, L. R.; Rose, N. J.; Abramson, E.; Caris, J. C . Synthesis and fluorescence of some trivalent lanthanide complexes. *J. Am. Chem. Soc.* **1964**, *86*, 5117−5125.
(23) Fernandes, M.; De, B. V.; Sa, F. R. A.; Carlos, L. D.; Charas, A.; Morgado, J.; Silva, M. M.; Smith, M. J. Highly photostable luminescent poly(ε-caprolactone)siloxane biohybrids doped with europium complexes. *Chem. Mater.* **2007**, *19*, 3892−3901.
(24) Rocha, L. A.; Caiut, J. M. A.; Messaddeq, Y.; Ribeiro, S. J. L.; Martines, M. A. U.; Freiria, J. d. C.; Dexpert-Ghys, J.; Verelst, M. Non-leachable highly luminescent ordered mesoporous SiO_2 spherical particles. *Nanotechnology* **2010**, *21*, 155603/1−155603/6.
(25) Khalilzadeh, P.; Lajoie, B.; El, H. S.; Furiga, A.; Baziard, G.; Berge, M.; Roques, C. Growth inhibition of adherent Pseudomonas aeruginosa by an N-butanoyl-L-homoserine lactone analog. *Can. J. Microbiol.* **2010**, *56*, 317−325.
(26) Zheng, Z.; Wang, J.; Liu, H.; Carducci, M. D.; Peyghambarian, N.; Jabbourb, G. E. A triboluminescent europium(III) complex. *Acta Crystallogr., Sect. C: Cryst. Struct. Commun.* **2002**, *C58*, m50−m52.
(27) Ye, Z.; Tan, M.; Wang, G.; Yuan, J. Preparation, characterization, and time-resolved fluorometric application of silica-coated terbium(III) fluorescent nanoparticles. *Anal. Chem.* **2004**, *76*, 513−518.
(28) Zhang, H.; Xu, Y.; Yang, W.; Li, Q. Dual-lanthanide-chelated silica nanoparticles as labels for highly sensitive time-resolved fluorometry. *Chem. Mater.* **2007**, *19*, 5875−5881.
(29) Xu, Y.; Li, Q. Multiple fluorescent labeling of silica nanoparticles with lanthanide chelates for highly sensitive time-resolved immunofluorometric assays. *Clin. Chem.* **2007**, *53*, 1503−1510.
(30) Note that the concentration of europium complexes in pure crystals, as has been calculated above for [Eu(TTA)$_3$(Bpy)], is less than 2 mmol cm^{-3}. The second estimation is based on the full coverage of a particle by complex units. With a 50 nm average diameter, the maximum number of complex units is 0.8 mmol cm^{-3} for one shell. Considering five shells, as described by the authors, this amounts to about 4 mmol cm^{-3}
(31) Malta, O. L.; Brito, H. F.; Menezes, J. F. S.; Goncalves, e. S. F. R.; Alves, S., Jr.; Farias, F. S., Jr.; de, A. A. V. M. Spectroscopic properties of a new light-converting device Eu-(thenoyltrifluoroacetonate)$_3$ 2(dibenzyl sulfoxide). A theoretical analysis based on structural data obtained from a sparkle model. *J. Lumin.* **1997**, *75*, 255−268.
(32) Nakamaru, K. Synthesis, luminescence quantum yields, and lifetimes of trischelated ruthenium(II) mixed-ligand complexes including 3,3′-dimethyl-2,2′-bipyridyl. *Bull. Chem. Soc. Jpn.* **1982**, *55*, 2697−2705.
(33) Zhao, H.; Su, W.; Luo, Y.; Ji, Y.; Li, Z.; Jiu, H.; Liang, H.; Chen, B.; Zhang, Q. Rectification of excitation with bathochromic shift induced by intense absorption of organic ligands during emission measurement of Eu(III) complex. *Spectrochim. Acta, Part A* **2006**, *65A*, 846−851.
(34) Aldeek, F.; Mustin, C.; Balan, L.; Roques-Carmes, T.; Fontaine-Aupart, M.-P.; Schneider, R. Surface-engineered quantum dots for the labeling of hydrophobic microdomains in bacterial biofilms. *Biomaterials* **2011**, *32*, 5459−5470.
(35) Rebek, J.; Feitler, D. Mechanism of the carbodiimide reaction. II. Peptide synthesis on the solid phase. *J. Am. Chem. Soc.* **1974**, *96*, 1606−1607.
(36) Kanno, S.; Yanagida, Y.; Haruyama, T.; Kobatake, E.; Aizawa, M. Assembling of engineered IgG-binding protein on gold surface for highly oriented antibody immobilization. *J. Biotechnol.* **2000**, *76*, 207−214.